Insight into replication effectiveness of laser-textured micro and nanoscale morphology by injection molding

Insight into replication effectiveness of laser-textured micro and nanoscale morphology by injection molding

Adrian H.A. Lutey[a*], Gianmarco Lazzini[a], Laura Gemini[b], Alexander Peter[c], Volkher Onuseit[c], Javier Graus[d], Francesco Fuso[e], Rainer Kling[b], Luca Romoli[a]

[a]Dipartimento di Ingegneria e Architettura, Università degli Studi di Parma, 43124 Parma, Italy

[b]ALPhANOV Centre Technologique Optique et Lasers, Talence 33400, France

[c]Institut für Strahlwerkzeuge, University of Stuttgart, 70569 Stuttgart, Germany

[d]BSH Electrodomésticos España S.A., 50016 Zaragoza, Spain

[e]Dipartimento di Fisica Enrico Fermi, Università di Pisa, 56127 Pisa, Italy

*Corresponding author: adrian.lutey@unipr.it

Abstract

Detailed analysis and characterization of injection-molded polypropylene (PP) specimens produced with laser-textured molds has been performed. Ultrashort pulsed laser surface structuring was exploited to produce sub-micrometric surface features on injection molds over areas of 2400 mm^2, including two-dimensional hole and cone arrays, and ridges parallel and perpendicular to the injection direction. Replication effectiveness was evaluated in terms of surface roughness parameters, Filling Volume Fraction (FVF) and Power Spectral Density (PSD), after which detailed comparison of the topography in the same region on plastic samples and molds was performed. A scatterometry setup was employed based on optical diffraction of a probe laser beam to assess replication fidelity over the entire surface of each PP sample with a measurement technique suitable for optimization and quality control in an industrial production environment. Of the tested surface morphologies, greatest replication effectiveness was achieved with LIPSS oriented parallel to the injection direction, where the arithmetic mean height of plastic samples (S_a = 37 ± 4 nm) was 97% of the corresponding value of the mold (S_a = 38 ± 6 nm), while the average FVF was 86±9% and the PSD indicated ripple-like features with a spacing of $\lambda \simeq 0.9$ μm. Direct comparison of the topography in selected regions highlighted local variability in the transfer effectiveness of individual surface features. The investigation demonstrated that micro and nanoscale morphology can effectively be transferred via injection molding over large areas relevant to industrial applications, while careful attention must be paid to the size and nature of defects in relation to the specific functional surface under consideration.

Keywords: Injection molding; Laser texturing; Ultrashort laser pulses; Replication; Nanoscale surface structures; Functional surfaces

1 Introduction

Micro and nanoscale morphology plays a fundamental role in the behavior of both natural and engineered functional surfaces [1]. Production of fine surface features has been exploited to modify wettability [2], ice adhesion [3], tribological performance [4], optical properties [5] and bacterial retention [6]. From a manufacturing point of view, the capacity to produce micro and nanoscale surface features over large areas represents a significant challenge in terms of production technology, throughput and cost. Amongst the various techniques employed to date, ultrashort pulsed laser irradiation has emerged as an important candidate

for texturing metallic surfaces due to its capability of producing surface features smaller than 1 μm via Direct Laser Interference Patterning (DLIP) [7] or Laser-Induced Periodic Surface Structures (LIPSS) [8]. In the former case, interference between a number of overlapping coherent laser beams leads to a periodic interference pattern on the target surface that depends on the optical configuration employed, with ablation taking place in zones where the local laser pulse fluence exceeds the threshold fluence [9]. In the latter case, interference between the incident laser beam and surface plasmon polaritons leads to the formation of parallel ridges perpendicular to the polarization orientation with a spatial period slightly smaller than the laser wavelength [10]. Laser textured hydrophilic and hydrophobic stainless steel and titanium alloy surfaces have been widely demonstrated in the literature [8]. A number of works have also demonstrated reductions in bacterial retention on stainless steel surfaces textured with ultrashort laser pulses for specific bacteria types such as *Escherichia coli* (*E. coli*) [6,11,12], *Staphylococcus aureus* (*S. aureus*) [12,13] and *Pseudomonas aeruginosa* (*P. aeruginosa*) [14]. Such reductions can be attributed to changes in wettability and a reduction in the available contact area for bacterial cells [15,16]. Despite this progress, the cost and throughput of ultrashort pulsed laser sources continue to be a major obstacle for the production of all but highly specialized products. The ability to transfer micro and nanoscale morphology from metallic molds to polymeric components with standard production processes would not only increase the range of materials that could exploit such surfaces, but also greatly improve productivity and economic feasibility [17].

The replication of micro and nanoscale surface structures on polymeric surfaces has been demonstrated with processes such as soft lithography, hot embossing and injection molding [18]. Soft lithography is effective at reproducing fine surface features below 100 nm but has limitations in terms of processing time and available materials. Low-cost superhydrophobic poly(dimethylsiloxane) (PDMS) surfaces have been produced via soft lithography with laser-textured molds characterized by LIPSS, increasing the static contact angle from 91° for flat PDMS to 157° for replicated samples with a 5 h solidification time [19]. This approach has been applied to improving the performance of PDMS microfluidic channels through creation of superhydrophobic inner channel walls, achieving increases in flow rate of up to 186% [20]. Superhydrophobic PDMS surfaces have also been achieved with larger surface features obtained via short and ultrashort pulsed laser ablation of molds and subsequent replication with curing times in the order of 1-3 h [21,22]. More recently, a reduction in *S. aureus* retention of approximately 82% was achieved following transfer of micro and nanoscale surface structures from ultrashort pulse laser textured Ti6Al4V surfaces to PDMS via soft lithography with a 24 h solidification period [11]. In this case, replication was quantified by comparing roughness parameters for the laser-textured and replicated surfaces. R_a, R_q and R_{pv} values were all found to be slightly lower on the replicated PDMS surfaces than on the textured mold, while peaks and valleys were generally similar in size or slightly smaller on the PDMS surface than on the molds. Roll-to-roll hot embossing is another viable method for replication of micro and nanoscale surface structures on polymeric films, providing greater throughput and flexibility in terms of materials. Embossing of polyethylene terephthalate (PET) films has been performed by texturing nickel sleeves with ultrashort pulsed DLIP to produce line structures with spatial wavelengths down to 1.5 μm and heights down to 141 nm, achieving similar transferred feature dimensions for web speeds of up to of 50 m/min [23].

For components with complex 3D geometry, injection molding with textured molds holds potential for producing functionalized surfaces based on replication of micro and nanoscale surface structures. Though texturing of molds with high precision can be achieved with relative ease, replication of micro and nanoscale surface features on thermoplastic polymers via injection molding remains an important challenge for manufacturers. Replication of microscale surface features in the order of 0.1-1 mm has been demonstrated on small polymeric samples on several occasions [24, 25]. While a number of studies have investigated the effects of LIPSS on polymer slip with the aim of reducing pressure requirements during injection molding [26,27], replication of micro and nanoscale structures has seen less attention in the literature. The effectiveness of replication is strongly dependent on parameters such as mold temperature, melt temperature, injection velocity and hold pressure, together with the design of the mold itself [28,29]. Injection molding of polypropylene (PP) with laser-textured molds has been demonstrated for a matrix of conical surface features of period ~13 μm and diameter ~5 μm produced by direct ablation with an ultrashort pulsed UV laser and diffractive optical element [30]. The resulting structures were found to increase the static water contact angle from approximately 90° for flat PP samples to approximately 160° for replicated samples. Similar results have also been achieved with mold inserts characterized by micro/nano arrays produced with UV lithography and ion etching [31]. The transfer of sub-micrometric ripple structures with a primary pitch distance of approximately 800 nm has instead been achieved through injection molding of polystyrene (PS) and poly(methyl methacrylate) (PMMA) using stainless steel molds textured with ultrashort laser pulses over circular areas of diameter 10 mm [32]. The replication of these structures was found to exhibit strong dependence on polymer viscosity and therefore mold temperature, with the replicated aspect ratio increasing with mold temperature up to approximately 80 % for PMMA and 65 % for PS at 120°C. Successful replication of LIPSS with a dominant wavelength of 650 nm and S_a of 21 nm has also been achieved via injection molding of PP over an area of approximately 100 mm^2, achieving ripple structures with a dominant wavelength of 610-620 nm and S_a of 10-13 nm depending on polymer crystallinity [17]. A smaller increase in contact angle compared to smooth samples was achieved in this case, which may have been due to the limited vertical dimensions of the transferred structures. The successful replication of sub-micrometric structures with laser-textured molds over small areas suggests injection molding has important potential for producing complex 3D polymer components with functional surfaces.

The present work involves detailed analysis and characterization of 60 mm × 40 mm × 2 mm injection-molded polypropylene samples produced with laser-textured molds, representing a larger replication area (2400 mm^2) than has previously been demonstrated for sub-micrometric surface structures. Replication effectiveness is also analyzed in greater detail than has been considered to date, providing new insight into transfer effectiveness both at a macroscopic scale and at the level of individual surface features. Ultrashort pulse DLIP and LIPSS are exploited to assess differences in replication effectiveness for surface structures characterized by different sub-micrometric geometries, including two-dimensional hole and cone arrays, and ridges parallel and perpendicular to the injection direction. Through comprehensive analysis of the resulting topography via Shear-Force Microscopy (ShFM), it is shown that despite comparable surface roughness parameters and an elevated Filling Volume Fraction (FVF, the ratio of replicated surface texture filling volume to that of the

mold), careful attention must be paid to the presence of micro-defects and their potential impact on the resulting surface functionality. Finally, scatterometry was employed to assess replication fidelity over the entire surface of each PP sample with a technique suitable for optimization and quality control in an industrial production environment.

2 Materials & Methods

2.1 Materials

The injection molds used for experiments were DIN 1.2344 (AISI H13 equivalent) tool steel with a Rockwell C hardness of 48-52. The molds were 105 mm × 60 mm × 20 mm in size with a 60 mm × 40 mm × 2 mm injection cavity, 10 mm fan injection gate and two 8 mm diameter ejection pins. The molds contained an internal circuit for circulation of heating water to avoid premature solidification of the plastic, ensure maximum replication of micro and nanoscale surface morphology and maintain constant temperature between production of different samples.

Injection molding experiments were performed with polypropylene homopolymer grade HB601WG supplied by Borealis. The polymer was specifically intended for injection molding and was characterized by a melt flow index of 2 g/10min at 230°C with a 16 kg load and an average shrinkage after injection of 1.4% as determined by the Borealis Method. Despite semi-crystalline polymers being less well-suited to replication of micro and nanoscale surface features, the choice of this material was based on its importance within the home appliances industry for production of components such as dishwasher tanks via injection molding, where there is strong interest in development of textured surfaces resistant to biofouling.

2.2 Laser texturing of molds with DLIP

Two molds were textured with DLIP using a custom setup based on a Duetto laser system from Time-Bandwidth Products AG. The laser was characterized by a wavelength of 1064 nm, pulse duration of 10 ps, repetition rate of 100 kHz and pulse energy of 29 µJ. The laser beam was delivered to a DLIP optical setup that split the laser into two beams and guided them back together at an angle of 74° (37° with respect to the mold surface normal). A detailed description of the setup, including a prediction model and parametric study, can be found in a previous work [33]. A line interference pattern with a spatial period of 880 nm was generated within the overlapping volume of the two coherent beams. By placing the metallic surface of the mold within this interference volume, ablation of parallel structures corresponding to the interference lines was achieved. The interference pattern cross section was 60 µm parallel to the feed direction and 190 µm perpendicular to the feed direction. With a feed rate of 100 mm/s parallel to the interference pattern, line structures with a period of 880 nm were produced. To achieve structuring of the entire surface, 190 µm wide line structures were generated adjacent to one another with a distance of 140 µm between the center of each line, denoted as the hatch distance. The mold was moved throughout the process while the DLIP setup was stationary to avoid vibration of the optical components or resulting interference pattern.

The above-mentioned procedure was repeated twice, rotating the mold 90° about the axis normal to the mold surface between each exposure. These two processing steps led to “cone” and “hole” structures on the molds, depending on the laser beam polarization

orientation with respect to the interference pattern. For cone structures, polarization of the laser beam was set perpendicular to the interference lines. Hole structures were instead generated by setting the polarization orientation parallel to the interference lines, generating a more complex pattern exploiting the super-positioning of DLIP and LIPSS. All other process parameters remained unchanged. Molds with cone and hole structures were denoted *mold A* and *mold B*, respectively. All relevant process parameters are summarized in Table 1.

Table 1: Process parameters employed for DLIP texturing of molds A and B

Repetition rate (kHz)	100
Average Power (W)	2.9
Feed rate (m/s)	0.1
Interference line period (nm)	880
Interference pattern cross section in feed direction (µm)	60
Interference pattern cross section perpendicular to feed direction (µm)	190
Hatch distance (µm)	140

2.3 Laser texturing of molds with LIPSS

A Tangerine laser system from Amplitude Système was employed to texture two additional metallic molds via LIPSS. The laser system was characterized by a wavelength of 1030 nm, pulse duration of approximately 300 fs, maximum deliverable average power of 20 W and a maximum repetition rate of 2 MHz. The output laser beam was directed through a beam expander before entering an IntelliSCAN14 galvanometric scanning head from ScanLAB, which could achieve a maximum scanning speed of 2 m/s. An f-theta lens with focal length of 100 mm was employed to focus the laser beam to a diameter of approximately 28 µm. Molds denoted *mold C* and *mold D* were textured with the same process parameters, presented in Table 2, but with different sample orientation with respect to the injection direction. For mold C, ripple orientation was parallel to the injection direction while for mold D, ripple orientation was perpendicular to the injection direction. The texturing parameters were chosen based on results presented in a previous work, where the antibacterial properties of laser-textured stainless steel samples were presented [12]. As the mold dimensions exceeded the working area of the galvanometric scanning head, a stitching procedure was carried out between two adjacent regions.

Table 2: Process parameters for LIPSS texturing of molds C and D

Repetition rate (kHz)	1000
Average Power (W)	0.8
Scanning speed (m/s)	2
Hatch distance between successive lines (µm)	5
Number of successive scans	1

2.4 Injection molding of plastic samples

Injection molding experiments were performed with an Arburg Allrounder 170S injection molding machine with a clamping force of 15 t, screw diameter of 22 mm and effective screw

length (L/D) of 20. Due to the risk of resistance to polymer flow and increased viscosity from rapid cooling upon contact with the micro and nanoscale surface structures on the laser-textured molds, emphasis was placed on maintaining polymer viscosity as low as possible during the mold filling stage. Optimization of injection molding parameters was performed with a series of preliminary experiments, leading to the final injection parameters presented in Table 3. These experiments were performed with a Design of Experiments (DoE) to optimize biofilm prevention on plastic samples. DOE factors included mass temperature (240-260 °C), mold temperature (25-80 °C), hold pressure (35-70 MPa) and volumetric flow rate (10-62 cm^3/s). A cooling time of 10 s was employed. The ejector speed was 200 mm/s with a force of 10kN. Due to the limited vertical extension of the micro and nanoscale morphology on the laser-textured molds, no demolding issues were observed during experiments and no extra release agent was required. A photograph of a laser-textured stainless-steel mold and plastic replica used for experiments is shown in Fig. 1.

Table 3: Injection molding parameters

Mass temperature (°C)	260
Back pressure (MPa)	2
Injection pressure (MPa)	30
Holding pressure (MPa)	45
Mold temperature (°C)	65
Volumetric flow rate (cm^3/s)	50

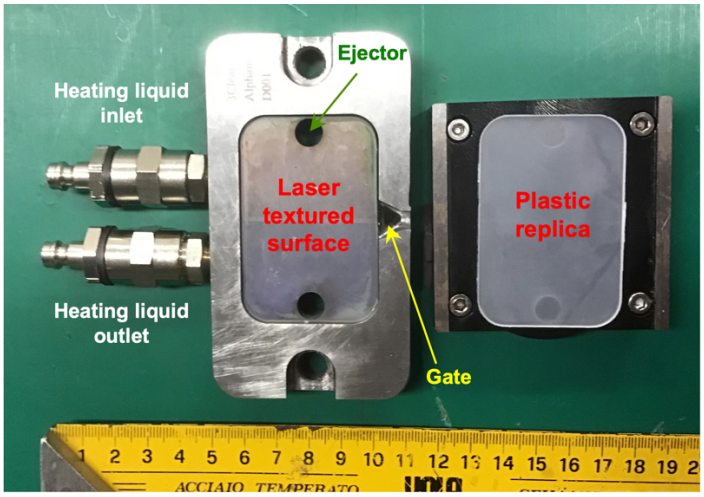

Figure 1: Photograph of laser textured stainless steel mold (left) and polypropylene replica sample (right).

2.5 Scanning electron microscopy

Molds textured with DLIP were analyzed with a JEOL JSM-6490LV scanning electron microscope (SEM). Molds textured with LIPSS were instead analyzed with a Tescan VEGA3 SEM. Selected injection-molded polypropylene samples were coated with 8 nm of gold and analyzed with a Phenom ProX desktop SEM using a secondary electron (SE) detector and a 10 kV electron beam.

2.6 Topography analysis

Correct characterization of the replication effectiveness and dimensional quality control required high accuracy topography measurements to be carried out [34-35]. Shear force microscopy (ShFM) was therefore performed to acquire the surface topography of two injection-molded plastic samples for each of the four molds. The surface topography of mold C was acquired with ShFM to provide reference data for evaluation of the texture transfer effectiveness on the respective injection-molded samples. The topography of mold C was considered as being representative of mold D, as both were produced with the same laser setup, process parameters and material, with only the mold orientation changed with respect to the laser scanning direction and polarization orientation. Reference data for molds A and B were instead taken from a previous study where surface structures were produced on flat steel samples with the same DLIP setup [33].

The ShFM scanning probe consisted of a 125 μm tungsten wire that was electrochemically etched to an apical diameter of approximately 50 nm. The probe was glued to the prong of a piezoelectric quartz tuning fork, which was maintained in oscillation at its fundamental natural frequency of approximately 32 kHz. A nano-positioner with horizontal resolution of 1 nm and vertical resolution of 0.1 nm (calibrated values) was employed with a feed-back control system to maintain the tip within a few nanometers of the surface and acquire the surface topography based on changes in the oscillation amplitude and phase induced by friction in the air layer between the surface and probe. Further to the nano-positioner resolution, measurement accuracy was affected by fluctuations due to acoustic and mechanical sources. In typical operating conditions, such fluctuations produced topographic noise below 2 nm as ascertained by scanning atomically flat reference samples. Positioning accuracy in subsequent scans and measurement repeatability were evaluated by scanning reference samples consisting of surface features produced by lithography, leading to an instrumental error on the order of a few nanometers in all scanning directions. Full details of the setup are presented in a previous work [36]. Scanning parameters were held constant with a tip scanning speed of 1-2 μm/s, acquiring maps over areas ranging from 10×10 μm^2 to 80×80 μm^2 consisting of up to 1024×1024 pixels. For plastic samples produced with molds C and D, specimen orientation within the instrument was chosen such that the fast scanning direction was orthogonal to the surface features (parallel ripples) within $\pm 3°$ to maximize sensitivity. For plastic samples produced with molds A and B, the fast scanning direction was approximately 45° to the features (square cones and holes). This setup enabled effects such as long-term drift within the reconstructed topography to be minimized. A total area of at least 6000 μm^2 was investigated for each sample by performing several ShFM scans over different areas. The resulting standard deviation of the derived roughness parameters, typically greater than the abovementioned instrumental accuracy, was used to determine measurement uncertainty.

2.7 Characterization of replication effectiveness

Following initial ShFM analysis, surface protrusions observed with greater height than the surrounding topography were analyzed in more detail over areas of 10×10 μm^2 on each sample. The spatial distribution of these protrusions, denoted *micro-burrs*, was evaluated by using a grain recognition algorithm based on a threshold method. The threshold was set to approximately 60% of the maximum height. The algorithm therefore identified structures having a closed shape with a projected area greater than 0.1 μm^2 and height above the

aforementioned threshold value. The occurrence of such features could potentially affect evaluation of areal surface roughness parameters by artificially increasing the measured roughness, thus leading to overestimation of the transfer effectiveness. Corrected roughness data were therefore generated by excluding identified micro-burrs to allow effective assessment of the replication process. The Power Spectral Density (PSD) was then calculated in the horizontal direction for specific ShFM topography maps to assess the correspondence between the predominant spatial wavelength on the molds and corresponding polymer samples.

Further to comparison of roughness parameters for each mold and plastic sample, a statistical method was employed to assess the quality of the replication process based on the Filling Volume Fraction (FVF) [37]. A watershed segmentation algorithm [38] was applied to the uncorrected ShFM topography maps to identify protrusion and ridge patterns on the molds and plastic samples, respectively. Algorithm parameters, embedded within the software employed for data analysis [39], were chosen to reject abnormal surface features such as micro-burrs in the plastic samples and scratches in the molds. Once patterns were identified, the filling volume for each mold (V_{mold}) and plastic sample (V_{sample}) was calculated based on ShFM data and the FVF determined as the ratio V_{sample}/V_{mold}.

2.8 Detailed analysis of replication effectiveness

A more precise analysis of micro and nanoscale replication effectiveness was performed through closer inspection of surface features on plastic samples and the same regions of the corresponding mold, allowing direct comparison of the surface texture obtained on the mold and replicated sample. This task required the ShFM tip to be positioned within a few μm of the same region on the plastic sample and stainless-steel mold. While the nano-positioners and optical imaging system theoretically allowed such accuracy, reliable reference points within the imaging system field of view were required. Careful inspection of the mold revealed the presence of a few macroscopic defects with an appropriate contrast in optical imaging, which were visibly replicated on the plastic substrate. Such defects were used as markers in positioning the ShFM tip to scan the same regions of the mold and replicated plastic samples.

2.9 Replication quality control in an industrial production environment

Finally, a simple scatterometry setup was employed based on optical diffraction of a probe laser beam to assess the fidelity of the replicated textures over the entire surface of each PP sample. Such a technique allows optimization and quality control of injection molded nanostructures in an industrial production environment, with measurement and processing times being shorter than a typical injection molding cycle [40-42]. A 473 nm laser beam with a diameter of 1.3 mm was directed onto the replicated plastic samples at normal incidence. Due to the presence of regular height variations, the samples behaved as optical diffraction gratings. Diffraction was observed in reflection as it was not possible to perform observations in transmission due to optical diffusion within the polymer. A reflected spot was detected with a power of approximately 1% of the incident beam. Only the first-order diffracted beam was considered as higher order diffraction peaks were very weak. The mapped diffraction intensity was intended to provide indirect information relating to the macroscopic quality and homogeneity of the transferred topography, as a local decrease in signal corresponded to a higher degree of disorder.

As with any diffraction grating, the angular dispersion depended on the spacing of the surface features. In the present case, a spacing in the range 0.84-0.90 μm and a probe laser wavelength of 473 nm led to an angular dispersion in the range 30-34°. The height and width of the diffraction peaks were convolved functions of several parameters, including the surface roughness and overall regularity of the pattern. In the experimental setup, the diffracted intensity was collected with a photodetector with an acceptance angle of ±1.5° about the nominal diffraction angle. Each sample was scanned over the entire surface to acquire the corresponding diffraction intensity. Scanning was performed in 0.1 mm steps for 42 mm in the direction corresponding to the short side of the samples and in 1 mm steps for 54 mm in the direction corresponding to the long side of the samples. Spatial resolution was dictated by the laser beam diameter, in the order of 1 mm in the present case. Since the diffraction signal was always superimposed on diffuse light from the sample surface, maps were normalized against the intensity in regions where no pattern was present.

3 Results and discussion

3.1 SEM analysis

SEM images of molds B and C are shown in Fig. 2 as examples of surfaces produced with the two laser texturing techniques employed. Horizontal feature spacing was in the order of 0.80-0.90 μm in all cases. DLIP holes were characterized by distinct, regularly spaced protrusions, while LIPSS presented a typical structure induced by single-beam irradiation of metallic surfaces with ultrashort laser pulses characterized by a series of parallel ridges and valleys. Distinct micro and nanoscale morphologies were observed in each case, allowing assessment of the transfer effectiveness of both one and two-dimensional laser-induced features via injection molding.

SEM images of injection-molded plastic samples produced with the same molds are presented in Fig. 3. In the case of DLIP holes, the replicated surface morphology was a series of cones with negative geometry compared to the mold used for its production (Fig. 2(a)). In the case of LIPSS, the replicated surface morphology had similar characteristics to the mold used for its production (Fig. 2(b)), with a series of parallel ridges and valleys. Individual defects such as micro-burrs resulting from the injection-molding process and subsequent sample extraction could be observed; however, these were relatively limited in extent. Qualitative analysis of the plastic surface therefore confirmed the possibility of replicating micro and nanoscale morphology on polypropylene via injection molding.

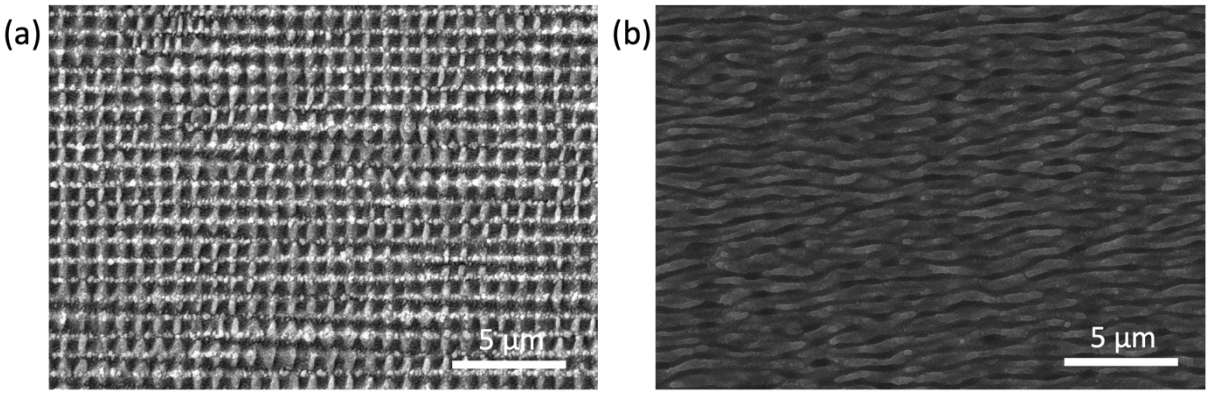

Figure 2: Scanning electron images of molds with DLIP holes (mold B) (a) and LIPSS (mold C) (b).

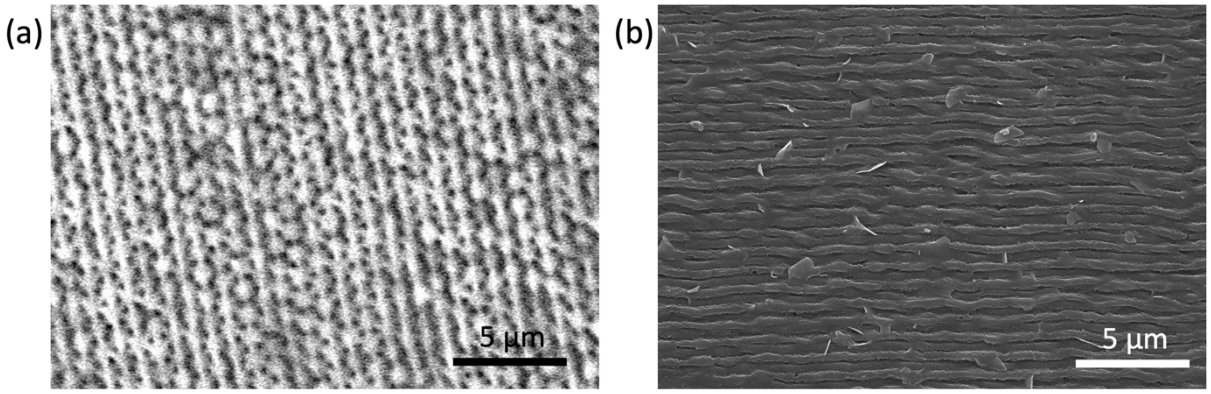

Figure 3: SEM images of injection-molded plastic samples produced with mold B (a) and mold C (b).

3.2 Topography analysis

Figure 4 shows representative 10 × 10 µm² topography maps of all tested injection-molded plastic samples together with the respective reference surfaces (Section 2.6). Areal surface parameters derived from several ShFM scans over different areas of each sample are summarized in Table 4. The expected features comprising cones, holes and ripples were consistently transferred; however, defects were detected in the form of linear scratches, micro holes and surface waviness, with consequent variations in average height. Furthermore, features not often found on laser textured stainless steel surfaces were also observed on plastic samples, including isolated protrusions exhibiting markedly greater height than the average topography. These micro-burrs were likely to have resulted from the injection-molding process itself and subsequent sample extraction.

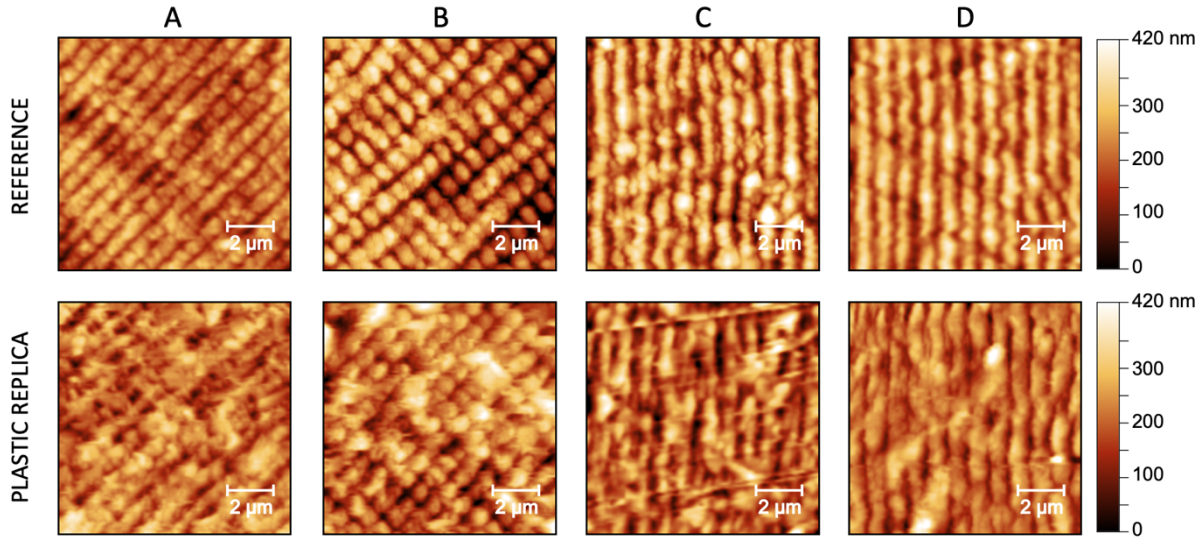

Figure 4: Representative 10 × 10 µm² topography maps of all reference and injection-molded plastic samples obtained via ShFM analysis.

Table 4: Areal surface roughness parameters derived for all injection-molded plastic samples. The prominent periodicity was determined through 2D autocorrelation maps. Reported

uncertainty intervals represent the dispersion of results obtained through statistical methods based on several ShFM acquisitions performed over different areas of each sample.

Quantity	Units	Sample A	Sample B	Sample C	Sample D
Prom. periodicity	λ [µm]	0.84 ± 0.02	0.84 ± 0.02	0.90 ± 0.02	0.89 ± 0.02
Arithmetic mean height	S_a [nm]	49 ± 4	52 ± 3	48 ± 3	44 ± 5
RMS height	S_q [nm]	61 ± 6	66 ± 4	61 ± 4	58 ± 5
Max. height	S_z [µm]	0.42 ± 0.05	0.45 ± 0.04	0.47 ± 0.04	0.43 ± 0.04
Max. peak height	S_p [µm]	0.19 ± 0.03	0.23 ± 0.04	0.29 ± 0.03	0.29 ± 0.03
Max. pit height	S_v [µm]	0.22 ± 0.03	0.21 ± 0.04	0.18 ± 0.02	0.14 ± 0.02

3.3 Characterization of replication effectiveness

With the aim of showing a typical example of the replication effectiveness, Figure 5(a) presents a detailed topography map of an area on plastic sample C exhibiting local protrusions. The corresponding line profiles show that these features are superimposed on the underlying texture, as their height is up to 100 nm above the average ripple height. Such features were typically observed in regions where the surface texture was characterized by a local irregularity such as the merging of two adjacent ripples. The features were also irregularly shaped due to coalescence of several topography peaks. While attempts were made to remove such features from the surface by using gentle cleaning procedures aimed at preventing texture damage such as soft air blowing and brief immersion in ethanol, no appreciable differences were observed. Taking into account their shape and spatial distribution, a possible interpretation for their formation may be the presence of micro-burrs resulting from detachment of the plastic substrate from the mold. While the extension of such defects was relatively limited, their presence may have affected evaluation of the areal surface parameters.

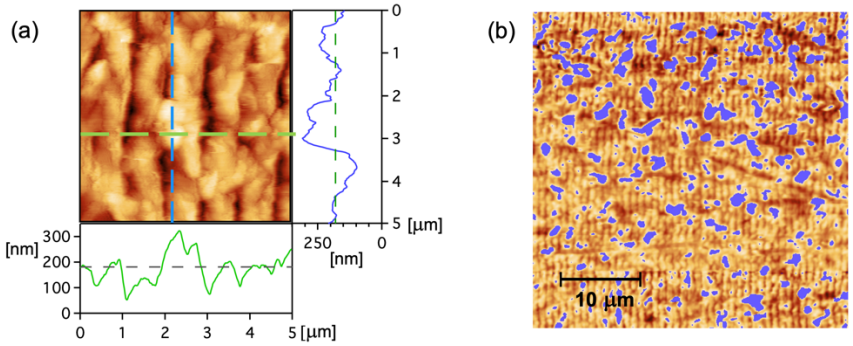

Figure 5: Detailed topography map of plastic sample C showing isolated protrusions with line profiles along the horizontal and vertical dashed segments (a); 40 × 40 µm^2 topography map of the same sample with blue spots representing micro-burrs identified with the grain recognition algorithm (b).

An example of the results of the developed recognition algorithm for identification of micro-burrs can be seen in Fig. 5(b) for sample C over an area of 40 × 40 µm^2, with protrusions identified as blue grains. The micro-burrs covered approximately 10-15% of the investigated region. It was observed that the micro-burrs were often distributed in stripes, possibly reflecting local inhomogeneities in injection-molding parameters such as temperature, pressure and composition. Corrected roughness data excluding the identified micro-burrs are

presented in Table 5, together with data from reference metallic samples. In this case, the average surface roughness of the plastic samples decreased by about 20%.

Assessment of the texture replication effectiveness was performed by comparing the areal surface roughness parameters of injection-molded plastic samples with those of the laser-textured molds used for their production. Reference data for molds A and B were obtained from a previous study using similar process parameters [33], while reference data relating to molds C and D were measured directly from mold C, which was produced with the same laser parameters as mold D. Table 5 reports a comparison of the measured roughness parameters for the reference samples and corrected values for the corresponding injection-molded plastic samples, where the effects of micro-burrs were removed. Discrepancies between the values for the mold and corrected values for the replicated plastic samples were limited in all cases, with differences typically within the range of experimental error.

Table 5: Comparison of corrected roughness data for injection-molded plastic samples and reference laser-textured steel surfaces. Reported uncertainty intervals represent the dispersion of results obtained through statistical methods based on several ShFM acquisitions performed over different areas of each sample.

Quantity	Units	Correct. Sample A	Ref. Mold A	Correct. Sample B	Ref. Mold B	Correct. Sample C	Correct. Sample D	Ref. Mold C/D
Arithmetic mean height	S_a [nm]	42 ± 4	55 ± 3	41 ± 3	67 ± 3	37 ± 4	34 ± 5	38 ± 6
RMS height	S_q [nm]	51 ± 6	61 ± 4	52 ± 4	79 ± 5	43 ± 4	41 ± 5	43 ± 7
Max. height	S_z [μm]	0.38 ± 0.05	0.42 ± 0.04	0.36 ± 0.04	0.54 ± 0.04	0.34 ± 0.04	0.32 ± 0.04	0.44 ± 0.12

The arithmetic mean height (S_a) of the corrected surface profiles of plastic samples A, B, C and D were 76%, 61%, 97% and 89% of the corresponding reference samples, respectively. Excluding the influence of micro-burrs, discussed previously, these results indicate that greatest replication effectiveness was achieved with LIPSS oriented parallel to the injection direction (sample C), followed by LIPSS oriented perpendicular to the injection direction (sample D), DLIP cones (sample A) and DLIP holes (sample B). This outcome is likely linked to polymer flow with respect to the textured mold surface morphology during the injection-molding processes. Micro and nanoscale structures exhibiting simple vertical features parallel to polymer flow facilitate effective replication, while more complex surface morphology or the presence of features perpendicular to the flow direction lead to a reduction in replication effectiveness. This outcome has important implications for the design of replicated functional surfaces, which must take into consideration both the required functionality and replication process.

Figure 6 compares the Power Spectral Density (PSD) calculated along the horizontal direction of ShFM topography maps of mold C and the corresponding replicated plastic sample. In this case, maps were averaged over 20 μm in the vertical direction. Further to other features stemming from waviness and large-scale features, peaks were clearly observed in both spectra. Taking into account their position, corresponding to a spatial frequency of $k = 2\pi/x \simeq 6.9$ μm^{-1}, in agreement with ripple-like features with spacing $\lambda \simeq 0.9$ μm, their occurrence can be attributed to the transferred texture. The peak height, representative of

the overall regularity of the textured patterns, was slightly lower for the replica sample suggesting a slightly higher degree of disorder.

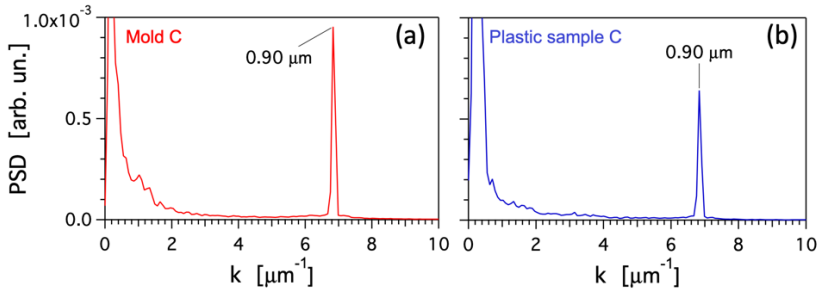

Figure 6: PSD calculated in the horizontal direction of ShFM topography maps for mold C (a) and the replicated polymer sample (b).

Figure 7 presents a schematic showing application of the watershed segmentation algorithm employed to evaluate the transfer effectiveness based on the Filling Volume Fraction (FVF), together with ShFM maps of mold C and the corresponding plastic sample highlighting the identified patterns in red and blue, respectively. FVF values were generally above 75% for all investigated samples, depending on the portion of the surface that was analyzed. For sample C, achieving the highest FVF, analysis was carried out over the same areas of both the mold and plastic samples. The complete scanned surfaces, around 10^4 µm^2 in area, were divided into square 20 x 20 µm^2 portions over which statistical methods were applied to accurately evaluate the FVF data and determine uncertainty. In terms of projected area, the patterns identified by the algorithm occupied similar fractions of the scanned mold (62±5%) and plastic sample (58±7%), indicating similarity between the spatial distribution of surface features on the two surfaces. Through calculation of the filling volume for the scanned mold and plastic sample within the identified regions, the FVF was determined as 86±9%.

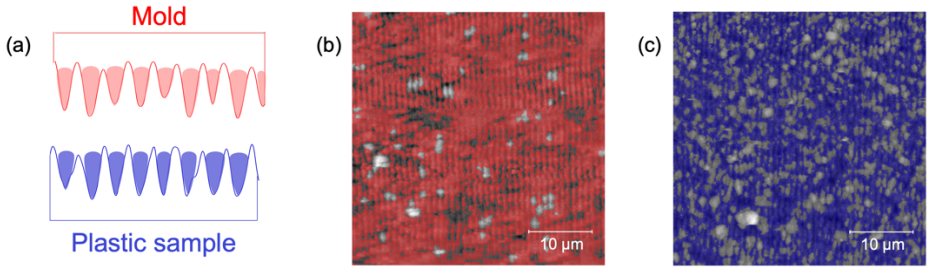

Figure 7: Schematic showing the cross section of the identified pattern volumes as shaded areas for calculation of the FVF (a); examples of patterns identified by the watershed segmentation algorithm, represented by red and blue areas in topography maps of mold C (b) and the corresponding plastic sample (c).

3.4 Detailed analysis of replication effectiveness

Mold C and the respective plastic samples were chosen for detailed analysis of replication effectiveness as LIPSS oriented parallel to the injection direction exhibited greatest macroscopic transfer effectiveness in terms of surface roughness parameters and FVF. Direct comparison of the topography in selected regions of the mold and samples was performed through closer inspection of surface features on the plastic samples and the same regions of the mold based on the presence of defects that were transferred to the plastic. Positioning accuracy in the direction normal to the LIPSS was <200 nm, while accuracy parallel to the

LIPSS was limited by the optical positioning system and was therefore approximately 2 µm. Line profile data were filtered with a low-pass filter with a cut-off spatial period of 4 µm to remove waviness observed on length scales larger than the texture periodicity. Furthermore, data pertaining to the replicated sample were inverted to match hills and valleys on the mold and replicated surface. The outcome of this analysis is shown in Fig. 8, where it can be observed that the ripple width was similar in both cases, with differences in the order of the measurement resolution, approximately 40 nm. The depth of the replicated features was somewhat variable, allowing direct assessment of the vertical transfer effectiveness of individual features.

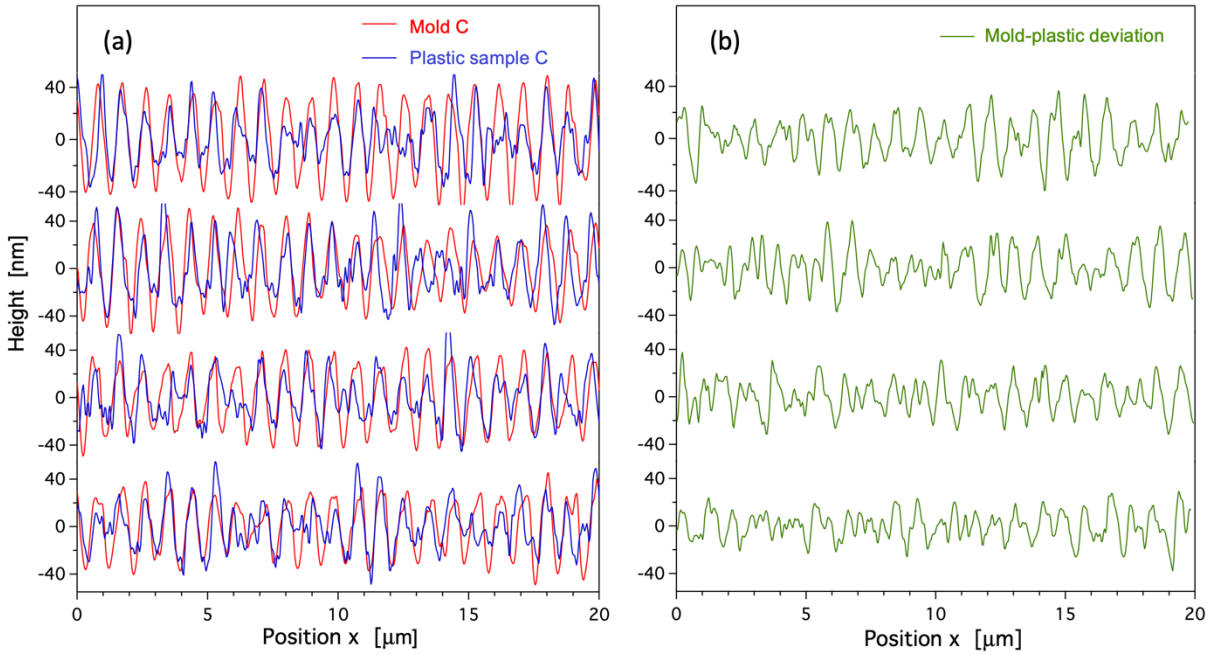

Figure 8: Comparison of selected line profiles for mold C and the corresponding injection-molded plastic sample (a) and point-to-point deviation between the two topography profiles (b).

Detailed analysis of the topography in the same region of the mold and replicated samples provided important insight into the accuracy with which individual surface structures could be replicated. While the spatial wavelength and average surface feature height were similar for both the mold and corresponding plastic surfaces, confirming findings relating to macroscopic characterization of replication effectiveness, it is clear from Fig. 8 that the transfer effectiveness of individual features exhibited significant local variability. While LIPSS on the mold surface were essentially regular, the replicated plastic surface exhibited regions of limited texture transfer, as well as regions in which the presence of defects led to greater peak-to-valley elevation than the original mold surface.

The implications of such local variations in the replication of micro and nano-scale defects must be carefully considered in relation to the specific functional surface under consideration. For modification of wettability, the presence of such defects is likely to enhance the hydrophilic or hydrophobic nature of the surface by increasing the Wenzel roughness factor [38]. For optical components, however, the presence of local variations and defects is likely to inhibit performance by reducing the ordered nature of surface features required to

produce optical gratings and waveguides. Effects on bacterial retention and biofilm formation are instead expected to depend on the size of variations or defects in relation to the micro-organism in question. Features smaller than the cell size enhance antibacterial and antibiofouling properties by limiting the available cell-substrate contact area, while those larger in size lead to the opposite effect by providing shelter from hydrodynamic turbulence [15]. The ability to identify the type, size and distribution of defects deriving from the replication process itself therefore represents an important tool in predicting and verifying surface functionality, for which further investigation into this aspect is required.

3.5 Replication quality control in an industrial production environment

An angular dispersion measurement obtained with the scatterometry setup employed for industrial replication quality control is illustrated in Fig. 9. Specifically, the diffracted intensity was computed as a function of the observation angle based on the Fraunhofer formula [39]. The topography pattern derived from ShFM line profiles of sample C was used as the diffraction source in the calculation, leading to the spectrum shown as a blue line in Fig. 9. For comparison, the spectrum obtained from a theoretically regular pattern of form $\sin^2(kx)$ with height comparable to the experimental S_z is reported as a green line in the same figure, exhibiting features purely due to diffraction. The occurrence of defects and the lower pattern regularity for the plastic sample resulted in a decrease in height of the main peak, along with a slight shift in diffraction angle and the presence of an unstructured background.

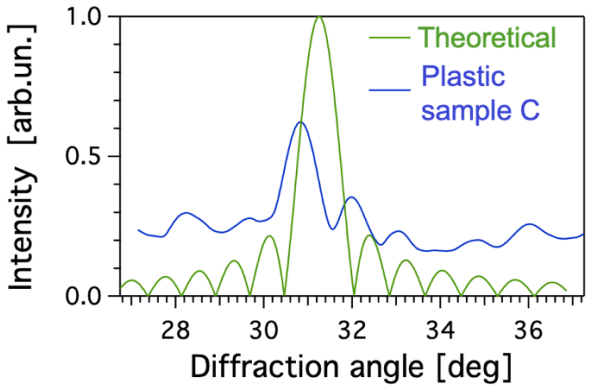

Figure 9: Computed diffraction intensity for a pattern derived from the ShFM line profile of sample C together with a theoretically regular pattern.

Figure 10 shows the acquired diffraction signal maps for plastic samples produced with molds C and D. The signal was not constant on the length scale considered, with variations in the order of 4-5× recorded between maximum and minimum values, suggesting some inhomogeneity in the replication process. This may have been due to local variations in process parameters or waviness of the molds themselves. On the other hand, a diffraction signal was observed on all of the investigated surfaces, demonstrating that the expected surface morphology was nonetheless transferred over a large area. By comparing the diffraction signal maps for both samples produced with molds characterized by LIPSS, it is interesting to note that despite the lower transfer effectiveness of sample D, exhibiting a lower diffraction signal intensity, the signal itself was more homogeneous over the entire surface implying a more uniform replication process for LIPSS oriented perpendicular to the injection direction than for LIPSS oriented parallel to the injection direction. The implications of this outcome again depend on the intended surface functionality. Although the method is

unable to discriminate between different effects that are possibly involved in lowering the diffracted power of the pattern, it represents a viable approach for a rapid and non-obtrusive investigation at a macroscale and therefore provides an effective approach for rapidly assessing the quality of replication over large surfaces in an industrial production environment. Further investigation is now required into discriminating factors affecting the diffracted power, particularly in relation to comparing the same local regions of molds and replicated samples.

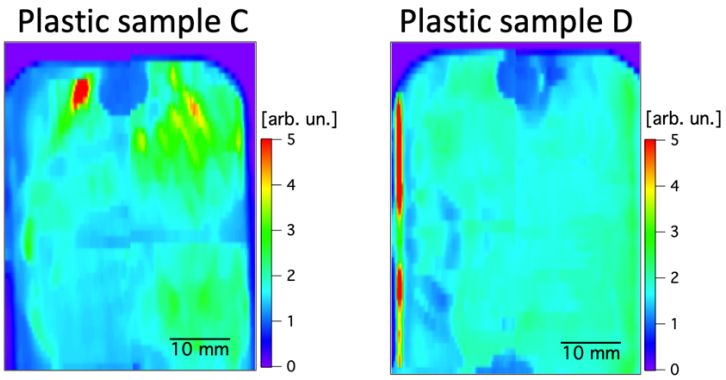

Figure 10: Diffraction signal maps for samples C and D.

4 Conclusion

Injection molding of 60 mm × 40 mm × 2 mm polypropylene samples has been performed using laser-textured molds with the aim of providing more comprehensive insight into replication effectiveness over an area of 2400 mm^2 based on analysis of the resulting topography based on ShFM. While replication of laser generated DLIP cones, DLIP holes and LIPSS oriented both parallel and perpendicular to the injection direction was demonstrated over the considered areas, differences in replication effectiveness were observed between the various surface morphologies, while local variations were observed between individual surface features on a given mold and plastic sample. Through comparison of areal roughness parameters and the FVF, best transfer effectiveness was achieved for LIPSS oriented parallel to the injection direction, following by LIPSS oriented perpendicular to the injection direction, DLIP cones and DLIP holes. In the first case, the arithmetic mean height of plastic samples (S_a = 37 ± 4 nm) was 97% of the corresponding value for the mold (S_a = 38 ± 6 nm), the average FVF was 86±9% and PSD measurements indicated ripple-like features with a spacing of $\lambda \simeq 0.9$ μm on both the mold and plastic sample. Detailed analysis of replication effectiveness through direct comparison of the topography in selected regions of the same mold and sample, however, highlighted local variability in the transfer effectiveness of individual surface features. Scatterometry based on angular dispersion measurements confirmed transfer effectiveness over large areas, indicating lower transfer effectiveness but greater homogeneity for LIPSS oriented perpendicular to the injection direction compared to LIPSS oriented parallel to the injection direction. While it is clear from the comprehensive analysis carried out that that effective replication of micro and nanoscale morphology from laser-textured molds to injection-molded polypropylene samples can be achieved over relatively large areas, the implications of local variations in replication effectiveness and micro and nano-scale defects must now be careful considered for further optimization and development of specific polymeric functional surfaces.

Acknowledgements

This project has received funding from the European Union's Horizon 2020 Research and Innovation Programme under Grant Agreement No. 687613.

References

[1] Elbourne A, Crawford RJ, Ivanova EP. Nano-structured antimicrobial surfaces: From nature to synthetic analogues. J Colloid Interf Sci 2017;508:603-16. https://doi.org/10.1016/j.jcis.2017.07.021.

[2] Feng L, Li S, Li Y, Li H, Zhang L, Zhai J, et al. Super-hydrophobic surfaces: From natural to artificial. Adv Mater 2002;14:1857-60. https://doi.org/10.1002/adma.200290020.

[3] Farhadi S, Farzaneh M, Kulinich SA. Anti-icing performance of superhydrophobic surfaces. Appl Surf Sci 2011;257:6264-9. https://doi.org/10.1016/j.apsusc.2011.02.057.

[4] Bieda M, Schmädicke C, Roch R, Lasagni A. Ultra-low friction on 100Cr6-steel surfaces after direct laser interference patterning. Adv Eng Mater 2015;17:102-8. https://doi.org/10.1002/adem.201400007.

[5] Dobrzański LA, Drygała A, Gołombek, K, Panek P, Bielańska E, Zięba P. Laser surface treatment of multicrystalline silicon for enhancing optical properties. J Mater Process Tech 2008;201:291-6. https://doi.org/10.1016/j.jmatprotec.2007.11.278.

[6] Epperlein N, Menzel F, Schwibbert K, Koter R, Bonse J, Sameith J, et al. Influence of femtosecond laser produced nanostructures on biofilm growth on steel. Appl Surf Sci 2017;418:420-4. https://doi.org/10.1016/j.apsusc.2017.02.174.

[7] Daniel C, Mücklich F, Liu Z. Periodical micro-nano-structuring of metallic surfaces by interfering laser beams. Appl Surf Sci 2003;208-209:317-21. https://doi.org/10.1016/S0169-4332(02)01381-8.

[8] Kietzig A-M, Hatzikiriakos SG, Englezos P. Patterned superhydrophobic metallic surfaces. Langmuir 2009;25:4821-7. https://doi.org/10.1021/la8037582.

[9] Lasagni AF, Roch T, Langheinrich D, Bieda M, Wetzig A. Large area direct fabrication of periodic arrays using interference patterning. Physcs Proc 2011;12;214-20. https://doi.org/10.1016/j.phpro.2011.03.125.

[10] Gnilitskyi I, Derrien TJ-Y, Levy Y, Bulgakova NM, Mocek T, Orazi L. High-speed manufacturing of highly regular femtosecond laser-induced periodic surface structures: physical origin of regularity. Sci Rep 2017;7:8485. https://doi.org/10.1038/s41598-017-08788-z.

[11] Rajab FH, Liu Z, Wang T, Li L. Controlling bacteria retention on polymer via replication of laser micro/nano textured metal mould. Opt Laser Technol 2019;111;530-6. https://doi.org/10.1016/j.optlastec.2018.10.031.

[12] Lutey AHA, Gemini L, Romoli L, Lazzini G, Fuso F, Faucon M, et al. Towards laser-textured antibacterial surfaces. Sci Rep 2018;8:10112. https://doi.org/10.1038/s41598-018-28454-2.

[13] Cunha A, Elie A-M, Plawinski L, Serro AP, Botelho do Rego AM, Almeida A, et al. Femtosecond laser surface texturing of titanium as a method to reduce the adhesion of *Staphylococcus aureus* and biofilm formation. Appl Surf Sci 2016;360:485-93. https://doi.org/10.1016/j.apsusc.2015.10.102.

[14] Fadeeva E, Truong VK, Stiesch M, Chichkov BN, Crawford RJ, Wang J, et al. Bacterial retention on superhydrophobic titanium surfaces fabricated by femtosecond laser ablation. Langmuir 2011;27:3012-9. https://doi.org/10.1021/la104607g.

[15] Whitehead KA, Verran J. The Effect of surface topography on the retention of microorganisms. Food Bioprod Process 2006;84:253-9. https://doi.org/10.1205/fbp06035.
[16] Helbig R, Günther D, Friedrichs J, Rößler F, Lasagni A, Werner C. The impact of structure dimensions on initial bacterial adhesion. Biomater Sci 2016;4:1074-8. https://doi.org/10.1039/C6BM00078A.
[17] Vera J, Brulez A-C, Contraires C, Larochette M, Valette S, Benayoun S. Influence of the polypropylene structure on the replication of nanostructures by injection molding. J Micromech Microeng 2015;25:115027. https://doi.org/10.1088/0960-1317/25/11/115027.
[18] Hansen HN, Hocken RJ, Tosello G. Replication of micro and nano surface geometries. CIRP Ann-Manuf Techn 2011;60:695-714. https://doi.org/10.1016/j.cirp.2011.05.008.
[19] Noh J, Lee J-H, Na S, Lim H, Jung D-H. Fabrication of hierarchically micro- and nano-structured mold surfaces using laser ablation for mass production of superhydrophobic surfaces. Jpn J Appl Phys 2010;49:106502. https://doi.org/10.1143/JJAP.49.106502.
[20] Sarbada S, Shin YC. Superhydrophobic contoured surfaces created on metal and polymer using a femtosecond laser. Appl Surf Sci 2017;405:465-75. https://doi.org/10.1016/j.apsusc.2017.02.019.
[21] Davaasuren G, Ngo C-V, Oh H-S, Chun D-M. Geometric study of transparent superhydrophobic surfaces of molded and grid patterned polydimethylsiloxane (PDMS). Appl Surf Sci 2014;314:530-6. https://doi.org/10.1016/j.apsusc.2014.06.170.
[22] Gong D, Long J, Jiang D, Fan P, Zhang H, Li L, et al. Robust and stable transparent superhydrophobic polydimethylsiloxane films by duplicating via a femtosecond laser-ablated template. ACS Appl Mater Interfaces 2016;8:17511-8. https://doi.org/10.1021/acsami.6b03424.
[23] Rank A, Lang V, Lasagni AF. High-speed roll-to-roll hot embossing of micrometer and sub micrometer structures using seamless direct laser interference patterning treated sleeves. Adv Eng Mater 2017;19:1700201. https://doi.org/10.1002/adem.201700201.
[24] Surace R, Bellantone V, Trotta G, Fassi I. Replicating capability investigation of micro features in injection moulding process. J Manuf Process 2017;28:351-61. https://doi.org/10.1016/j.jmapro.2017.07.004.
[25] Gamonal-Repiso P, Sánchez-Soto M, Santos-Pinto S, Maspoch ML. Improvement of the replication quality of randomly micro-textured injection-moulding components using a multi-scale surface analysis. J Manuf Process 2019;42:67-81. https://doi.org/10.1016/j.jmapro.2019.04.010.
[26] Sorgato M, Masato D, Lucchetta G, Orazi L. Effect of different laser-induced periodic surface structures on polymer slip in PET injection moulding. CIRP Ann-Manuf Techn 2018;67:575-8. https://doi.org/10.1016/j.cirp.2018.04.102.
[27] Orazi L, Sorgato M, Piccolo L, Masato D, Lucchetta G. Generation and characterization of laser induced periodic surface structures on plastic injection molds. Laser Manuf Mater Process 2020;7:207-21. https://doi.org/10.1007/s40516-020-00115-1.
[28] Lin H-Y, Chang C-H, Young W-B. Experimental and analytical study on filling of nano structures in micro injection molding. Int Commun Heat Mass 2010;37:1477-86. https://doi.org/10.1016/j.icheatmasstransfer.2010.08.017.
[29] Baruffi F, Gülçür M, Calaon M, Romano J-M, Penchev P, Dimov S, et al. Correlating nano-scale surface replication accuracy and cavity temperature in micro-injection moulding using in-line process control and high-speed thermal imaging. J Manuf Process 2019;47:367-81. https://doi.org/10.1016/j.jmapro.2019.08.017.

[30] Bekesi J, Kaakkunen JJJ, Michaeli W, Klaiber F, Schoengart M, Ihlemann J, et al. Fast fabrication of super-hydrophobic surfaces on polypropylene by replication of short-pulse laser structured molds. Appl Phys A-Mater 2010;99:691-5. https://doi.org/10.1007/s00339-010-5719-8.
[31] Weng C, Wang F, Zhou M, Yang D, Jiang B. Fabrication of hierarchical polymer surfaces with superhydrophobicity by injection molding from nature and function-oriented design. Appl Surf Sci 2018;436:224-33. https://doi.org/10.1016/j.apsusc.2017.11.268.
[32] Piccolo L, Sorgato M, Batal A, Dimov S, Lucchetta G, Masato D. Functionalization of plastic parts by replication of variable pitch laser-induced periodic surface structures. Micromachines 2020;11:429. https://doi.org/10.3390/mi11040429.
[33] Peter A, Lutey AHA, Faas S, Romoli L, Onuseit V, Graf T. Direct laser interference patterning of stainless steel by ultrashort pulses for antibacterial surfaces. Opt Laser Technol 2020;123:105954. https://doi.org/10.1016/j.optlastec.2019.105954.
[34] Tosello G, Hansen HN, Marinello F, Gasparin S. Replication and dimensional quality control of industrial nanoscale surfaces using calibrated AFM measurements and SEM image processing. CIRP Ann 2010;59:563-8. https://doi.org/10.1016/j.cirp.2010.03.141.
[35] Calaon M, Hansen HN, Tosello G, Garnaes J, Nørregaard J, Li W. Microfluidic chip designs process optimization and dimensional quality control. Microsyst Tecnol 2015;21:561-70. https://doi.org/10.1007/s00542-013-2025-3.
[36] Tantussi F, Vella D, Allegrini M, Fuso F, Romoli L, Abul C, et al. Shear-force microscopy investigation of roughness and shape of micro-fabricated holes. Precis Eng 2015;41:32-9. https://doi.org/10.1016/j.precisioneng.2015.01.003.
[37] Lee B-K, Hwang CJ, Kim DS, Kwon TH. Replication quality of flow-through microfilters in microfluidic lab-on-a-chip for blood typing by microinjection molding. J Manuf Sc E-T ASME 2008;130:021010. https://doi.org/10.1115/1.2896142.
[38] Kaestner A, Lehmann E, Stampanoni M. Imaging and image processing in porous media research. Adv Water Resour 2008;31:1174-87. https://doi.org/10.1016/j.advwatres.2008.01.022
[39] Nečas D, Klapetek P. Gwyddion: an open-source software for SPM data analysis. Cent Eur J Phys 2012;10:181-8. https://doi.org/10.2478/s11534-011-0096-2.
[40] Calaon M, Madsen MH, Weirich J, Hansen HN, Tosello G, Hansen PE, et al. Replication fidelity assessment of large area sub-µm structured polymer surfaces using scatterometry. Surf Topogr 2015;3:045005. https://doi.org/10.1088/2051-672X/3/4/045005.
[41] Madsen MH, Hansen P-E. Scatterometry-fast and robust measurements of nano-textured surfaces. Surf Topogr 2016;4:023003. https://doi.org/10.1088/2051-672X/4/2/023003.
[42] Madsen JS, Thamdup LH, Czolkos I, Hansen PE, Johansson A, Garnaes J, et al. In-line characterization of nanostructured mass-produced polymer components using scatterometry. J Micromech Microeng 2017;27:085004. https://doi.org/10.1088/1361-6439/aa7a3a.
[38] Bico J, Tordeux C, Quéré D. Rough wetting. Europhys Lett 2001;55:214-220. https://doi.org/10.1209/epl/i2001-00402-x.
[39] Hecht E, Zając A. Optics. 3rd ed. Massachusetts: Addison-Wesley; 1998.